Theoretical and Applied Climatology (2020) 139:261–274
https://doi.org/10.1007/s00704-019-02970-1

ORIGINAL PAPER

The changes of high-temperature extremes and their links with atmospheric circulation over the Northern Hemisphere

Lisuo Hu[1,2,3] · Gang Huang[2,3,4]

Received: 17 December 2018 / Accepted: 5 August 2019 / Published online: 14 August 2019

Abstract

The present study investigated the changes of high-temperature extremes and their links with atmospheric circulation over the Northern Hemisphere during 1979–2012 based on daily records of maximum temperature and geopotential height fields. We mainly used the 90th percentile of daily maximum temperatures as a threshold to identify hot day. The number of hot days (NHD) shows significant increasing trends over the East Asia (EA), Mediterranean (TM), and United States of America (USA) from 1979 to 2012, suggesting that these regions may suffer from increasing high-temperature extremes The regional mean linear trend over EA is 0.18 days/year and showed an increase in 1996, with the maximum trends in Mongolian Plateau and Loess Plateau. In the TM region, NHD increased with a rate of 0.35 days/year and showed an increase in 1997, and most significant trend was found in the Arabian Peninsula. In the USA, the NHD had a significant inter-annual variability and increased with a rate of 0.1 days/year. Moreover, high-temperature extremes over most parts of the three regions are associated with barotropical anticyclonic anomalies and subsidence, which may enhance solar radiation to surface.

1 Introduction

High-temperature extremes have a significant impact on economic and social activities, affecting the consumption of electricity and water and inducing the forest fires, crop losses, and heat-related working costs (Valor et al. 2001; Peng et al. 2004; Coumou and Rahmstorf 2012; Zhao et al. 2016). In addition, prolonged exposure to high-temperature extremes can lead to heat-related illnesses, including heatstroke, heat exhaustion, heat cramps, and respiratory diseases (Leechiong and Stitt 1995; Luber and McGeehin 2008), and result in an increase in mortality, especially in the elderly (Diaz et al. 2002).

✉ Gang Huang
hg@mail.iap.ac.cn

[1] State Key Laboratory of Satellite Ocean Environment Dynamics, Second Institute of Oceanography, Ministry of Natural Resources, Hangzhou, China

[2] State Key Laboratory of Numerical Modeling for Atmospheric Sciences and Geophysical Fluid Dynamics, Institute of Atmospheric Physics, Chinese Academy of Sciences, Beijing, China

[3] University of Chinese Academy of Sciences, Beijing, China

[4] Laboratory for Regional Oceanography and Numerical Modeling, Qingdao National Laboratory for Marine Science and Technology, Qingdao, China

Climate change has the potential to increase the frequency and magnitude of heat waves (Meehl and Tebaldi 2004). The twenty-first century has already featured a number of serious heat waves with negative impacts on crop production and human health (Kovats and Hajat 2008; Battisti and Naylor 2009; Dole et al. 2011). In August 2003, 22,000–35,000 heat-related deaths (14,800 in France) were caused by the heat wave that took place across Europe (Bouchama 2004; Schar and Jendritzky 2004). In the summer 2010, Moscow suffered a heat wave with unprecedented high mean temperature in July (Dole et al. 2011). In the more recent 2013 heatwave over China, over 5600 heat-related illnesses were reported, roughly two times more than in the previous years (Gu et al. 2016; Zhao et al. 2016). According to the World Meteorological Organization (WMO 2013), compared to the number of deaths due to heat waves (6000) in the decade before (1991–2000), the number (136,000) increased rapidly (by 2300%) during the most recent decade (2001–2010). And even after excluding the 2003 heat wave in European and 2010 heat wave in Russian, the THE-related deaths increased by 800%, which is much larger than the overall increase of 20% due to various extreme weather events including heat, cold, drought, storms, and floods.

In addition, global temperature is very likely to continue rising in the foreseeable future (Hansen et al. 2006; IPCC 2013). Temperature extremes have been studied on global,

regional, and national scales (You et al. 2011). The frequency of global heat wave has increased in the second half of the twentieth century (Easterling et al. 2000; Alexander et al. 2006). There is a remarkable consistency among the results obtained from previous studies which focus on regional and national scales. For example, hot days and warm nights showed an increasing tendency at most stations over the Asia-Pacific region (Choi et al. 2009). Dynamical model projections show increases in the frequency, intensity, and duration of temperature extremes over at least the next century (Kharin et al. 2007; Perkins et al. 2013).

Temperature extreme events are often accompanied by prominent anomalies in atmospheric circulation and precipitation, as well as in the conditions of the nearby land and ocean surfaces. The extreme 2003 European and 2010 Russian heat waves have been shown to be associated with blocking (Dong et al. 2016). Surface weather conditions are closely governed by the large-scale circulation of the Earth's atmosphere (Horton et al. 2015). Although a substantial portion of the observed change in extreme temperature occurrence has resulted from regional and global scale thermodynamic changes, the risk of extreme temperatures over some regions has also been altered by recent changes in frequency, persistence, and maximum duration of regional circulation patterns (Horton et al. 2015).

Although temperature extremes in most land regions show robust increasing trends, the pattern of change has not been spatially uniform. So it is reasonable to display the changes of temperature extremes globally and compare the differences and similarities over various regions. The objective of this study is to quantify changes of temperature extremes over the Northern Hemisphere during 1979–2012 and analyze spatial and temporal features of hot day in details over typical regions chosen according to the climatology and trend of hot day over the Northern Hemisphere. Moreover, we discuss possible relationship between temperature extremes and atmospheric circulation. The rest of this paper is organized as follows. Section 2 introduces the data and method. Section 3 describes climatology and change of high-temperature extremes over the Northern Hemisphere. Section 4 discusses the high-temperature extremes over sub-regions and their links with atmospheric circulation. Finally, discussions and conclusions are given in Section 5.

2 Data and method

2.1 Data

The records of daily maximum temperature are from the WATCH-Forcing-Data-ERA-Interim (WFDEI) climate dataset (Weedon et al. 2014). This dataset has the advantage of a high spatiotemporal resolution (at 0.5° × 0.5° resolution for the global land surface and at sub-daily/daily time steps for the period of 1979–2012) and a wide use for land surface modeling forcing (Zhao et al. 2015). This dataset was generated by applying bias correction to the ERA-Interim reanalysis product (Dee et al. 2011), following the same methodology implemented for the widely used WATCH Forcing Data (WFD) (Weedon et al. 2011). WFDEI includes a correction of T using the Climate Research Unit TS3.1/TS3.101 dataset (CRU) (Mitchell and Jones 2005). Else, Previous studies analyzed extreme temperatures based on WFDEI dataset both in global (Zhao et al. 2015) and regional (Zhao et al. 2016) scale and indicated that WFDEI is better than ERA-Interim in characterizing extreme temperatures in China (Hu et al. 2018).

The daily height fields and monthly reanalysis data are derived from the European Centre for Medium-Range Weather Forecasts Interim Reanalysis (ERA-Interim) (Dee and Uppala 2009) with a resolution of 0.5° × 0.5°, which is available from 1979 forward, but the analyzed time period is from 1979 to 2012. The ERA-Interim is the latest global atmospheric reanalysis produced by the European Centre for Medium-Range Weather Forecasts (ECMWF) and has substantial improvements compared to ERA-40 in many aspects, such as the representation of the hydrological cycle, the quality of the stratospheric circulation, and the consistency in time of the reanalysis fields (Dee et al. 2011).

2.2 Method

Two widely used indicators are chosen in present investigation to characterize the extreme temperature: absolute index and percentile index. The absolute index considers 35 °C of daily maximum temperature as a threshold to define extreme temperature. Besides, the records of daily maximum temperature from 1981 to 2010 in June, July, and August are ranked in an ascending order, and then the 90th percentile (TX90) is chosen from the order as a percentile threshold. The present study defines a hot day when the daily maximum temperature exceeds the threshold and emphatically analyzes the spatial and temporal features of the number of hot day (NHD).

Linear regression and empirical orthogonal function (EOF) are used applied to analyze long-term variations of the NHD, and Student's t test is used to examine the significance of linear regression. In addition, since regime shifts are defined as rapid reorganizations of ecosystems from one relatively stable to another, decadal shifts are detected by a method developed by Rodionov (2004) based on a sequential t test (details of regime shift detection are provided by NOAA, available at https://www.beringclimate.noaa.gov/regimes/#userconsent#).

To examine the relationship between the spatial and temporal variability of the summer (June–August (JJA) mean) atmospheric circulation and extreme temperature, we perform a singular value decomposition (SVD) analysis on the summer 200 hPa

height field and simultaneous NHD from 1979 to 2012 (details of the SVD method are provided on the NCAR Command Language (NCL) website at http://www.ncl.ucar.eud/).

3 Climatology and changes of high-temperature extremes

Figure 1 shows the climatology of NHD based on absolute index and the distribution of 90th percentile values of daily maximum temperature over the Northern Hemisphere from 1981 to 2010. The regions with frequent hot days based on absolute index mainly reside in North Africa and West Asia, with the NHD close to 90 days/JJA (Fig. 1a). The large values mean that almost all the days in whole summer are hot. These areas are located in tropical or subtropical regions where the surfaces are mainly composed of desert with scanty rainfall. Besides, Western USA is another domain where hot days frequently occur, especially in the west coast. It is evident from Fig. 1b that 90th percentile of daily maximum temperature displays a zonal structure with increasing first and then decreasing with the latitude from equator to the North Pole. The spatial features of TX90 are consistent with the climatology of NHD based on the absolute index, with larger values over subtropical regions, especially over North Africa and West Asia, and the maximum of TX90 in Sahara and the Arabian Peninsula.

The NHD based on absolute index increased in most part of the Northern Hemisphere from 1979 to 2012 and had most significant increasing trends over subtropical regions (Fig. 2a), especially in the Mediterranean, Caspian Sea region, and the USA, with values more than 6 days/10 years. However, over the major parts of Sahara and the Arabian Peninsula where hot days frequently occur, the trends of NHD are not significant (Fig. 2a). As the NHD in these regions is close to or more than 90 days in summer (92 days in total), the absolute index fails to display the changes of extreme temperature there. Figure 2b shows the linear trends of NHD based on percentile index over the Northern Hemisphere during 1979–2012. Significant increasing trends are seen in most parts of subtropical region and the most significant positive trends are seen in the Mediterranean and West Asia, especially in the Arabian Peninsula with trends more than 8 days/10 years. Compared to trends based on absolute index, East Asia is another region of significant trends based on the percentile index. In addition, percentile index magnifies the information of extreme temperature over Polar Regions, such as the significant increasing in Greenland (Fig. 2b).

Thus, absolute index is not proper for analyzing the trends over Sahara and the Arabian Peninsula, and it fails to reflect the extreme temperature in middle and high latitude where the NHD above 35 °C is 0. These problems are resolved when the analysis is based on percentile index that can reflect the extreme high temperature objectively. Percentile index is more comparable across different climatic regions, so the following analysis focuses on the results based on percentile index.

According to the climatology and tendency of NHD over the Northern Hemisphere, three sub-regions are chosen to do more detailed analysis: East Asia (EA) (30–55° N, 90–125° E),

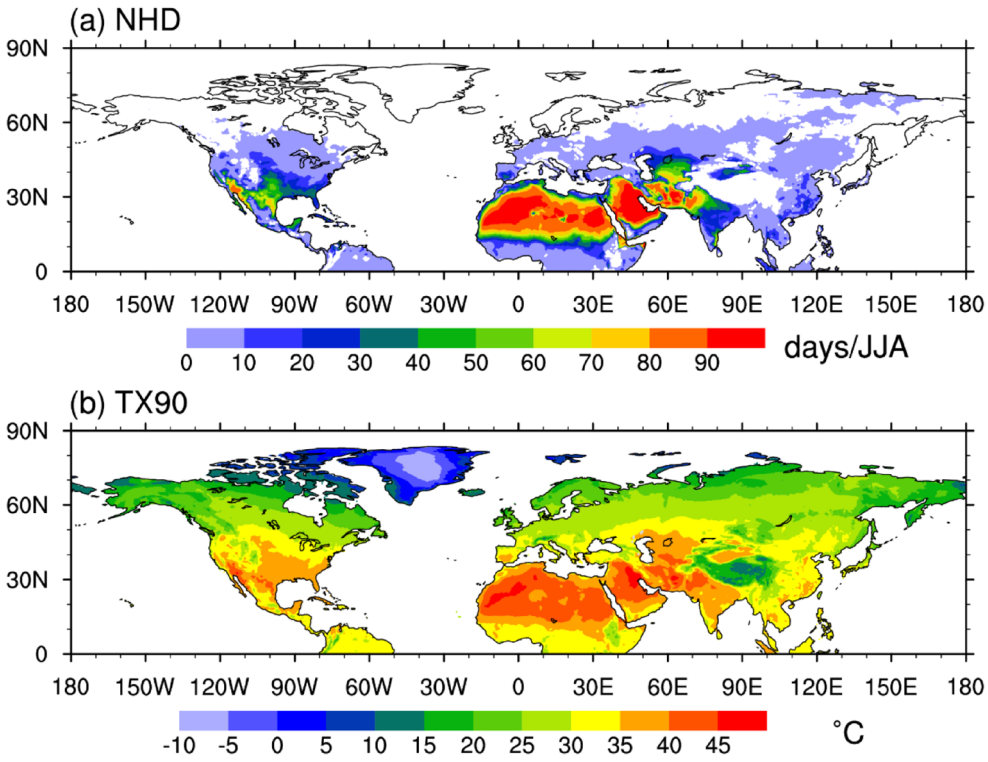

Fig. 1 Climatology of the NHD (units: days/JJA) based on absolute index (**a**) and distribution of 90th percentile (units: °C) values of daily maximum temperature (**b**) over the Northern Hemisphere

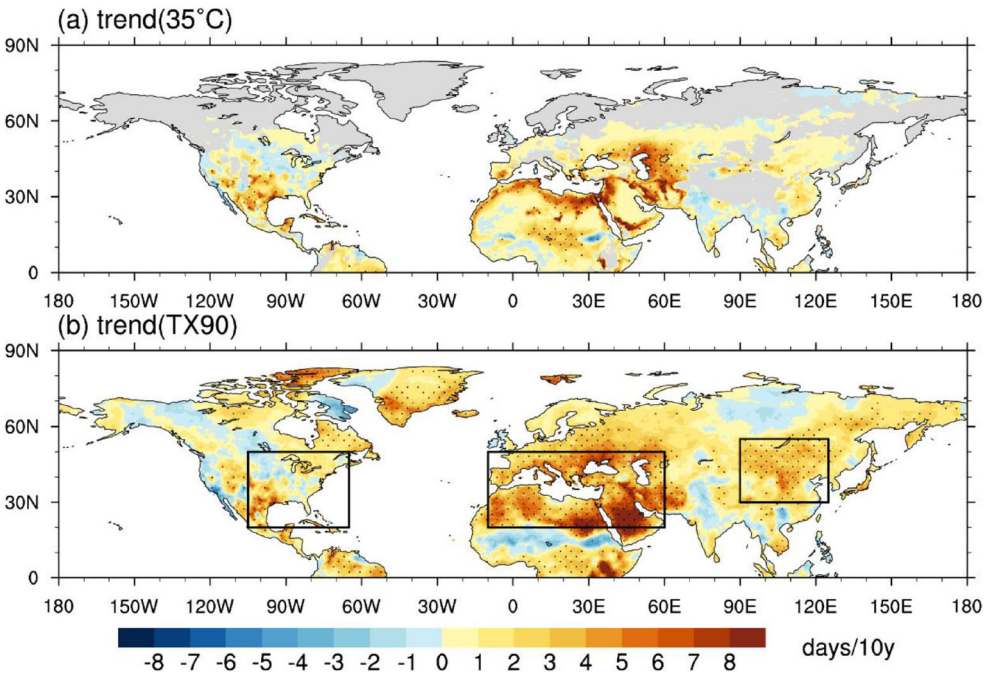

Fig. 2 Linear trends of NHD based on the absolute index (**a**) and percentile index (**b**) during 1979–2012 over the Northern Hemisphere, the point signs denote the grid points where the trend is significant at 99% confidence level according to Student's *t* test. The rectangular black boxes from left to right denote the regions that are chosen as the United States of America (USA), Mediterranean (TM), and East Asia (EA), respectively

Mediterranean (TM) (20–50° N, 10° W–60° E), and the USA (20–50° N, 105–65° W), and the scopes of the three sub-regions are depicted in Fig. 2b. These three sub-regions are selected because they are the areas where extreme temperature frequently occurs and exhibits significant increasing trends of NHD.

To investigate the main spatial and temporal features of NHD over the Northern Hemisphere, we show the first two EOF modes and corresponding principal components for the NHD based on percentile index from 1979 to 2012 in Fig. 3. The two modes explain about 20.2% and 7.3% of the total variance, respectively.

As Fig. 3a shows, the first leading EOF mode is characterized by uniform positive anomalies in the most parts of the Northern Hemisphere, and the corresponding PC (Fig. 3b) mainly features increasing trend. The EOF1 and PC1 indicate that NHD based on percentile index was depicted by negative anomalies from 1979 to 1997 and positive anomalies from 1997 to 2012. Hence, the NHD increased over the Northern Hemisphere, especially in North Africa and West Asia. The three sub-regions chosen above are the areas where NHD shows a significant variation according to the first leading EOF mode.

Additionally, the second leading EOF mode (Fig. 3c) shows a seesaw NHD pattern between the USA, East Europe, North Asia, and the other parts of the Northern Hemisphere. The second principal component (Fig. 3d) depicts negative phases from 1979 to 2000 and positive phases from 2000 to 2012 mainly. Thus, in the USA, East Europe, and North Asia, the NHD based on percentile index was above normal during 1979–2010 and below normal during 2000–2012, while the patterns reversed in the other parts of the Northern Hemisphere.

4 High-temperature extremes over sub-regions and their links with atmospheric circulation

Atmospheric general circulation is a direct factor which causes extreme high events. For example, the serious heat wave in Europe in 2003 from May to August is partly due to persistent anticyclonic conditions (Black et al. 2004). To examine the relationship between the atmospheric circulation and NHD, linear trends have been subtracted to remove long time-scale variations. For a 34-year time series, a correlation coefficient of 0.44 reaches the 99% confidence level based on the Student's *t* test.

Correlations of NHD with height fields in each grid over the Northern Hemisphere during 1979–2012 are shown in Fig. 4. Apparently, the distribution of correlation coefficient is remarkably similar between two pressure levels, but the coefficients of NHD with 500 hPa height field are larger than with 200 hPa. Significant positive correlation appears in major parts of the Northern Hemisphere, with positive centers in middle and high latitudes. This suggests a potential link between the NHD based on percentile index and anomalous height fields. Over the three sub-regions chosen above, the correlation coefficients between NHD and geopotential height are significant.

4.1 East Asia

The regional averaged NHD in the EA region increased with a linear trend of 0.18 days/year and showed a decadal increase via binomial 9a sliding average (red line) (Fig. 5a). Regime

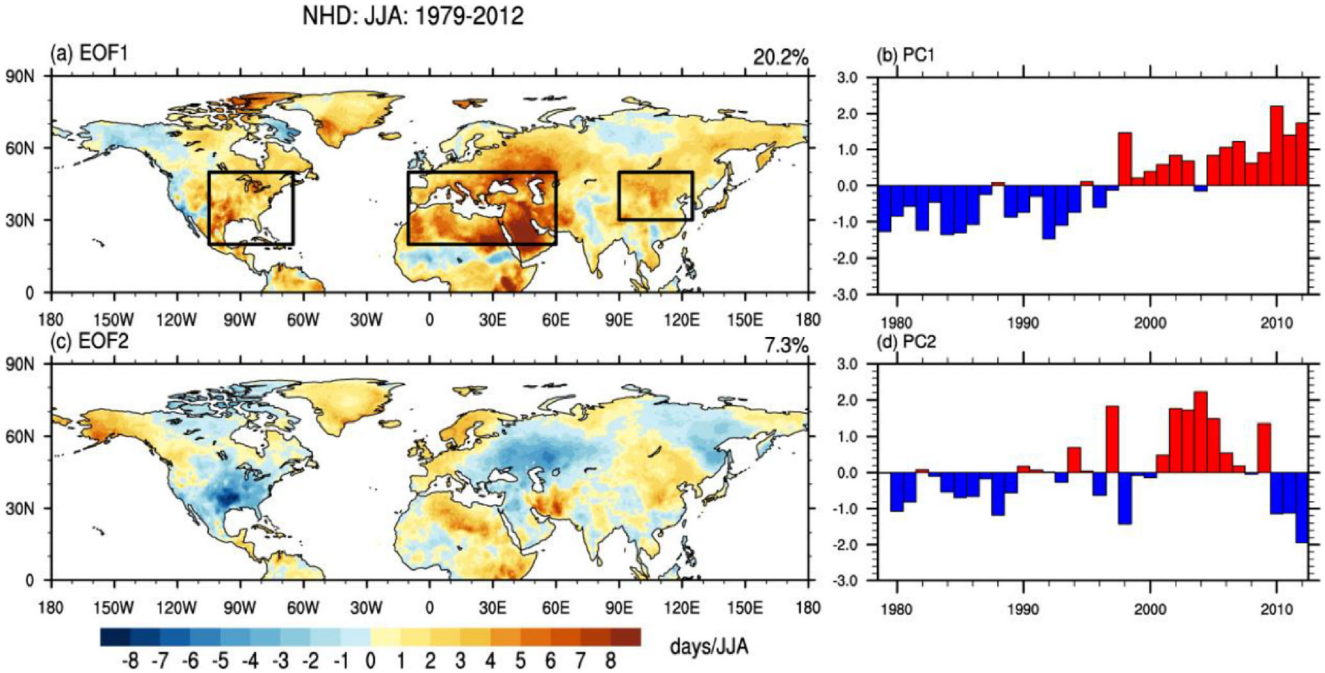

Fig. 3 The first EOF mode (**a**) and second EOF mode (**c**) of NHD based on percentile index over the Northern Hemisphere and the first principal component (**b**) and second principal component (**d**) during 1979–2012. The rectangular black boxes from the left to the right denote the regions that are chosen as the United States of America (USA), Mediterranean (TM), and East Asia (EA), respectively

shift detection indicates that regional NHD over EA had a regime shift in 1996. Therefore, the period is divided into two periods: low NHD period (pre-period: 1979–1996) with 9.11 days/JJA and high NHD period (post-period: 1997–2011) with 15.73 days/JJA. Averaged NHD patterns during 1979–1996, 1997–2011, and difference between two periods

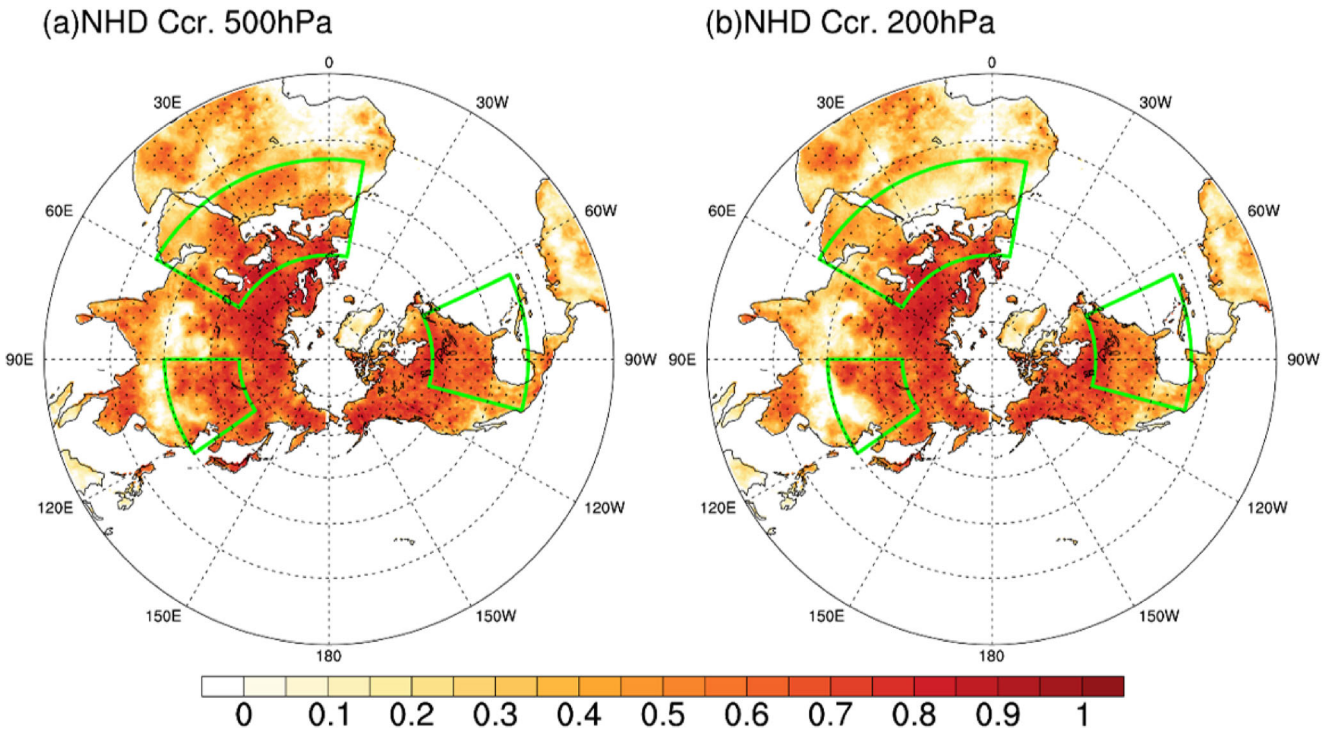

Fig. 4 Correlation coefficients of NHD based on percentile index with 500 hPa (**a**) and 200 hPa (**b**) height fields respectively from 1979 to 2012 over the Northern Hemisphere. The point signs denote the grid points where the correlation is significant at 99% confidence level according to Student's *t* test. Green arc areas from 150° W to east indicate the regions of the United States of America (USA), Mediterranean (TM), and East Asia (EA), respectively

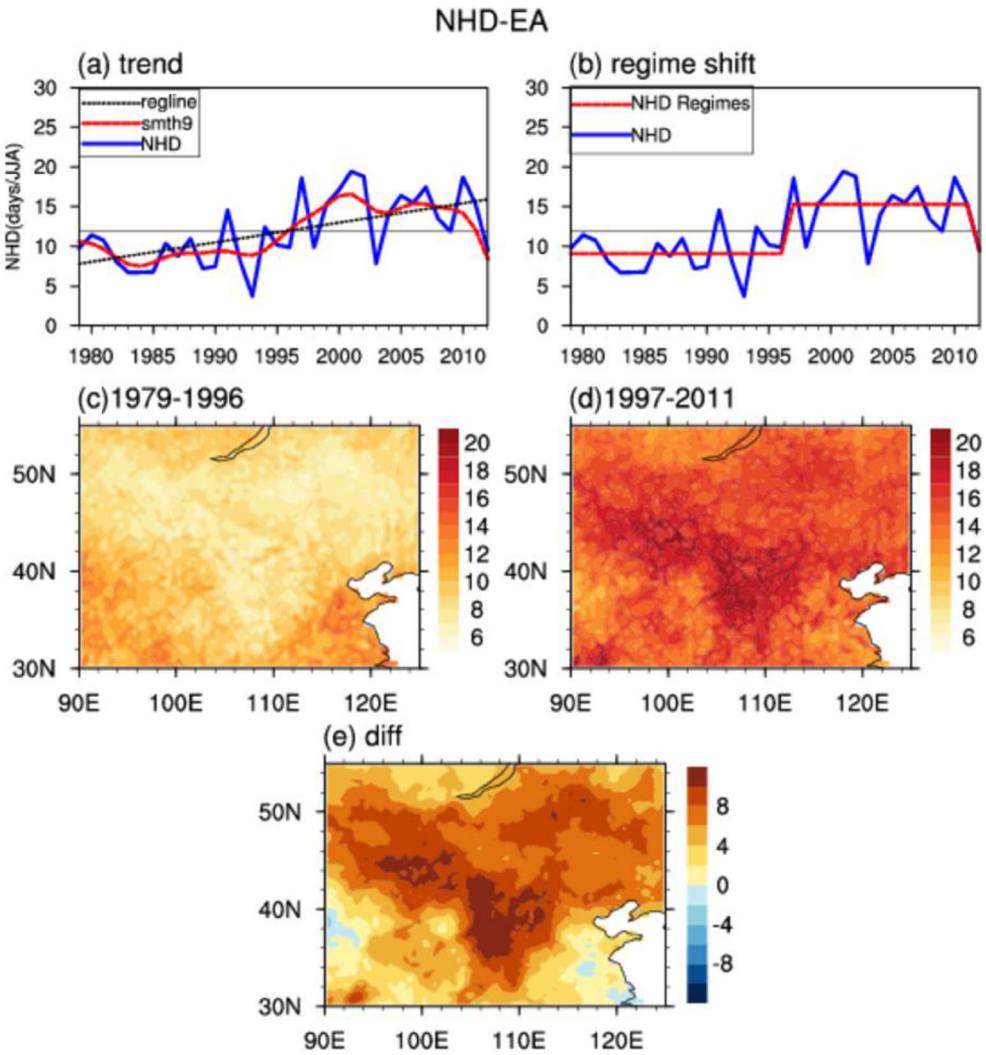

Fig. 5 Changes (**a**) and a regime shift (**b**) of the regional averaged NHD based on percentile index and averaged NHD during 1979–1996 (**c**), 1997–2011 (**d**) and difference between two periods (**e**) in the EA region

over EA are shown in Fig. 5c–e, respectively. From the pre-period to post-period, an increasing trend was found over most parts of EA, especially around the Mongolian Plateau and Loess Plateau.

To find out the atmospheric circulation associated with the decadal shift of NHD in the EA region, the differences of atmospheric circulation and downward shortwave radiation between two periods are shown in Fig. 6. There is an anomalous anticyclone during the post-period compared with pre-period in both the upper and lower troposphere over the most parts of EA (Fig. 6a, c). Associated with the anticyclonic anomalies, there are subsidence at 500 hPa (Fig. 6b) and downward shortwave radiation anomalies in the surface, which may heat air temperature indirectly through heating surface soil temperature.

The first and second SVD modes on the summer 200 hPa geopotential height field and simultaneous NHD from 1979 to 2012 are shown in Fig. 7, aiming at analyzing the correlation between the atmospheric circulation and extreme temperature over the EA. The first two modes explain about 92.1% and 5.7% of the total variance, indicating that the first mode is the main pattern.

The first homogeneous SVD modes (Fig. 7a, b) are characterized by positive height anomalies with maximum center at the latitude around 45° N and remarkable above-normal NHD around the Mongolian Plateau and Loess Plateau, consistent with the most significant increases of NHD (Fig. 5e). The correlation coefficient between the two corresponding principal components (PCs) is 0.86, suggesting a close relationship between geopotential height and NHD. There is an evident change that the values of standardized PCs are mainly below zero during 1979–1995 and above zero during 1996–2012 (Fig. 7c). Therefore, anticyclonic anomalies and above-normal NHD over the EA mainly appear during 1996–2010, while cyclonic anomalies and below normal NHD mainly appear during 1979–1995. The second SVD mode indicates a dipole pattern of anomalies of 200 hPa geopotential height and NHD between north part and south part of EA (Fig. 7d, e), and the correlation of PCs is 0.77 (Fig. 7f). Else, the inter-annual variability of PCs is significant.

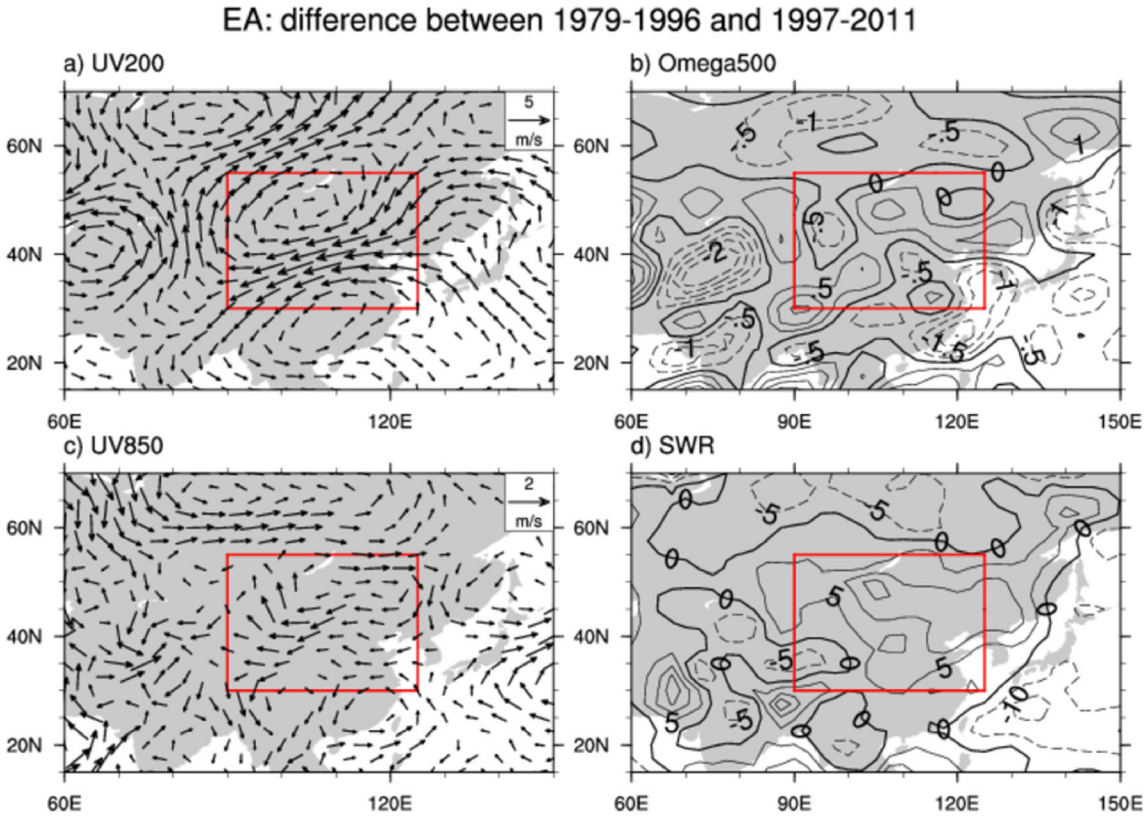

Fig. 6 Differences of (**a**) 200-hPa wind (units: m/s), (**b**) 500-hPa vertical pressure velocity (dp/dt) (units: 10^{-4} hPa/s), (**c**) 850-hPa wind (units: m/s), and (**d**) surface downward shortwave radiation (units: W/m^2) between 1997–2011 and 1979–1996 in the EA region. The red rectangular boxes denote the regions that are chosen as the EA

4.2 Mediterranean

Figure 8 shows the changes of NHD in the TM region. The regional mean NHD in the TM shows an increasing trend during 1979–2012 (linear trend valued 0.35 days/year). Specifically, there is a gradual increasing trend from 1979 to 1990s and a prominent increasing trend from 1990s to 2012 (Fig. 8a). A regime shift of regional NHD in 1997 is detected, with 9.74 days/JJA during 1979–1997 (pre-period) and 18.74 days/JJA during 1998–2012 (post-period). Areas where hot days frequently occurred are located in the Western Sahara during 1979–1996 and in the Arabian Peninsula during 1997–2012 (Fig. 8c, d). From the pre-period to the post-period, an increasing trend was found over the whole TM region, especially around the Arabian Peninsula.

Figure 9 shows the differences of atmospheric circulation and downward shortwave radiation between pre-period and post-period. The whole TM had a regime increasing shift of NHD in 1997, but the factors for this shift are different in the north part and south part of TM (Fig. 9). Over the north part (from 40° N to north), there is an anomalous anticyclone during the post-period compared with pre-period in both the upper and lower troposphere over the north part of TM (Fig. 9a, c), and subsidence anomalies occur at 500 hPa (Fig. 9b), resulting from the anomalous high pressure. Meanwhile, downward shortwave radiation in the surface demonstrates a positive anomaly (Fig. 9d), favoring the occurrence of extreme heat. Over the south part (from 40° N to south), there is ascent at 500 hPa, and downward shortwave radiation decreased. Harpaz et al. (2014) indicated that horizontal advection is the dominant factor in the occurrence of HETs in the eastern Mediterranean region, but not the warming associated with subsidence.

The first and second SVD modes on the summer 200 hPa geopotential height and simultaneous NHD from 1979 to 2012 are shown in Fig. 10, and the first two modes explain about 89.9% and 3.0% of the total variance, respectively, suggesting that the first mode is the dominant mode. As Fig. 10a, b shows, the first homogeneous SVD mode indicates a positive geopotential height and hot days anomalies over the TM. NHD is above normal when the TM region is controlled by positive height anomalies, with a localized maximum NHD around the Arabian Peninsula. The correlation of PCs is 0.77 (Fig. 10c). The second SVD mode is characterized by a see-saw pattern of geopotential height and NHD between western and eastern TM, with a localized minimum over Sahara region (Fig. 10d, e). The correlation of PCs is 0.74, suggesting a close relationship between the 200 hPa geopotential height and NHD, and the PCs show a significant inter-annual variability (Fig. 10f).

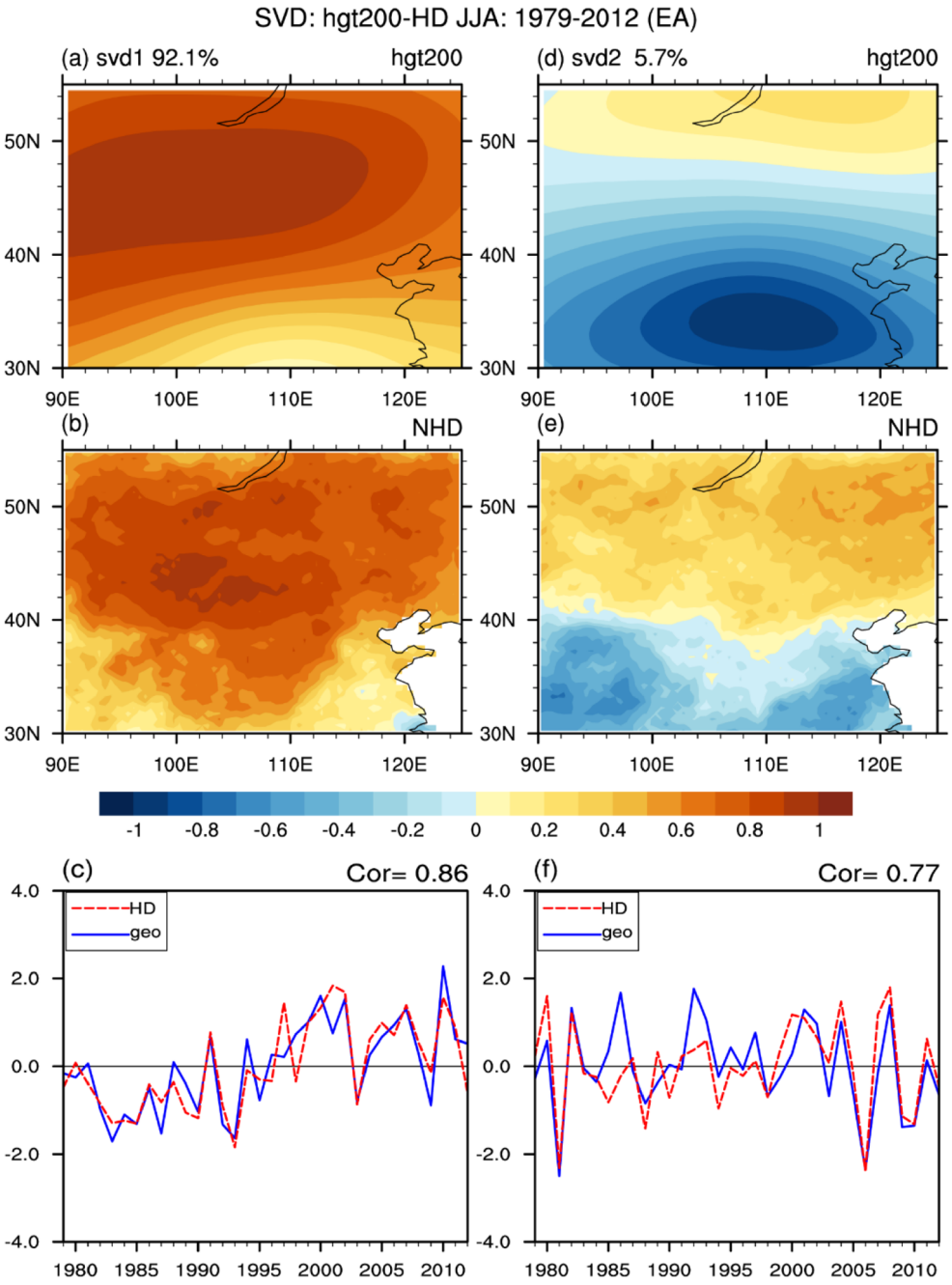

Fig. 7 First (**a**–**c**) and second (**d**–**f**) leading SVD homogeneous correlation map of summer 200-hPa height field (**a**, **d**) and simultaneous NHD (**b**, **e**) over the EA region and standardized homogeneous time series of first (**c**) and second (**f**) leading SVD mode. SVD analysis is based on the data from 1979 to 2012

4.3 United States of America

The changes of regional NHD over the USA display an interannual variation with a linear trend of 0.1 day/year (Fig. 11a). We define hot years when the standardized anomaly of regional NHD is larger than 1.0, and cold years when the standardized is smaller than − 1.0. Hence, hot years over the USA are chosen including 1980, 1983, 1988, 1995, 1998, 2005, 2006, 2010, 2011, and 2012, while cold years including 1979, 1982, 1984, 1985, 1992, 1994, 1996, 1997, 2000, and 2004 (Fig. 11b). Over the USA, the most significant difference between hot years and cold years was in the west of the Mississippi River (Fig. 11c, d, f).

Figure 12 displays the difference of atmospheric circulation and downward shortwave radiation between hot years and cold years. Comparing to cold years, there is an anomalous anticyclone in both the upper and lower troposphere over the USA region in hot years (Fig. 12a, c), and subsidence anomalies occur at 500 hPa (Fig. 12b), resulting from the anomalous high pressure. Cloud is inhibited due to subsidence, favoring extreme temperature through enhancing solar radiation at the surface (Fig. 12d).

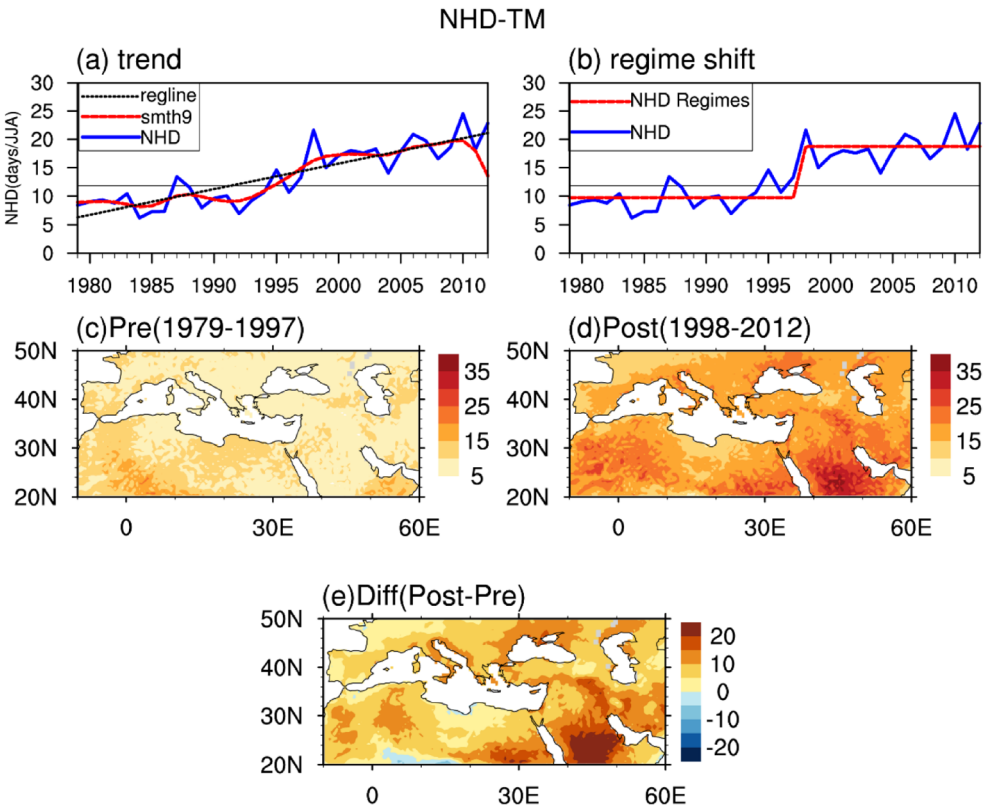

Fig. 8 Changes (**a**) and a regime shift (**b**) of the regional averaged NHD based on percentile index and averaged NHD during 1979–1997 (**c**), 1998–2012 (**d**), and difference between two periods (**e**) in the TM region

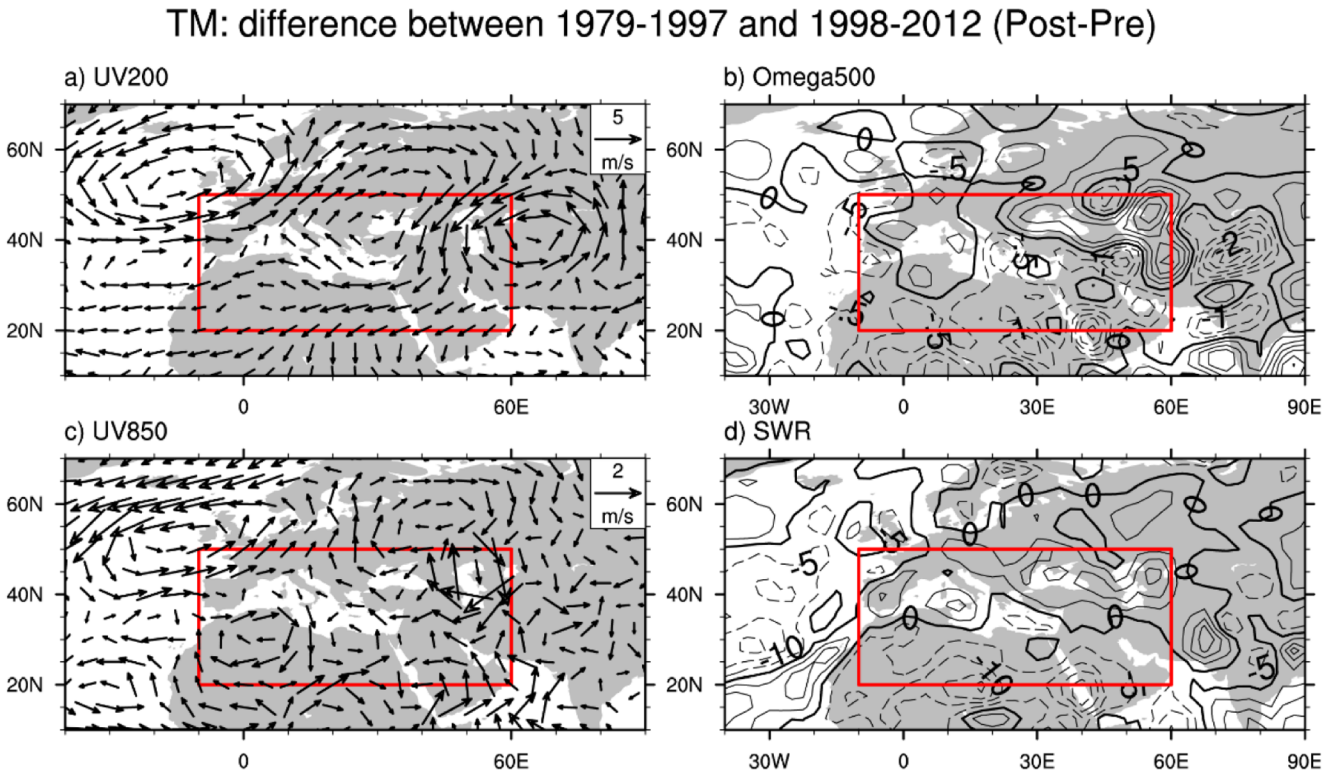

Fig. 9 Differences of (**a**) 200-hPa wind (units: m/s), (**b**) 500-hPa vertical pressure velocity (dp/dt) (units: 10^{-4} hPa/s), (**c**) 850-hPa wind (units: m/s), and (**d**) surface downward shortwave radiation (units: W/m^2) between 1998–2012 and 1979–1997 in the TM region. The red rectangular boxes denote the regions that are chosen as the TM

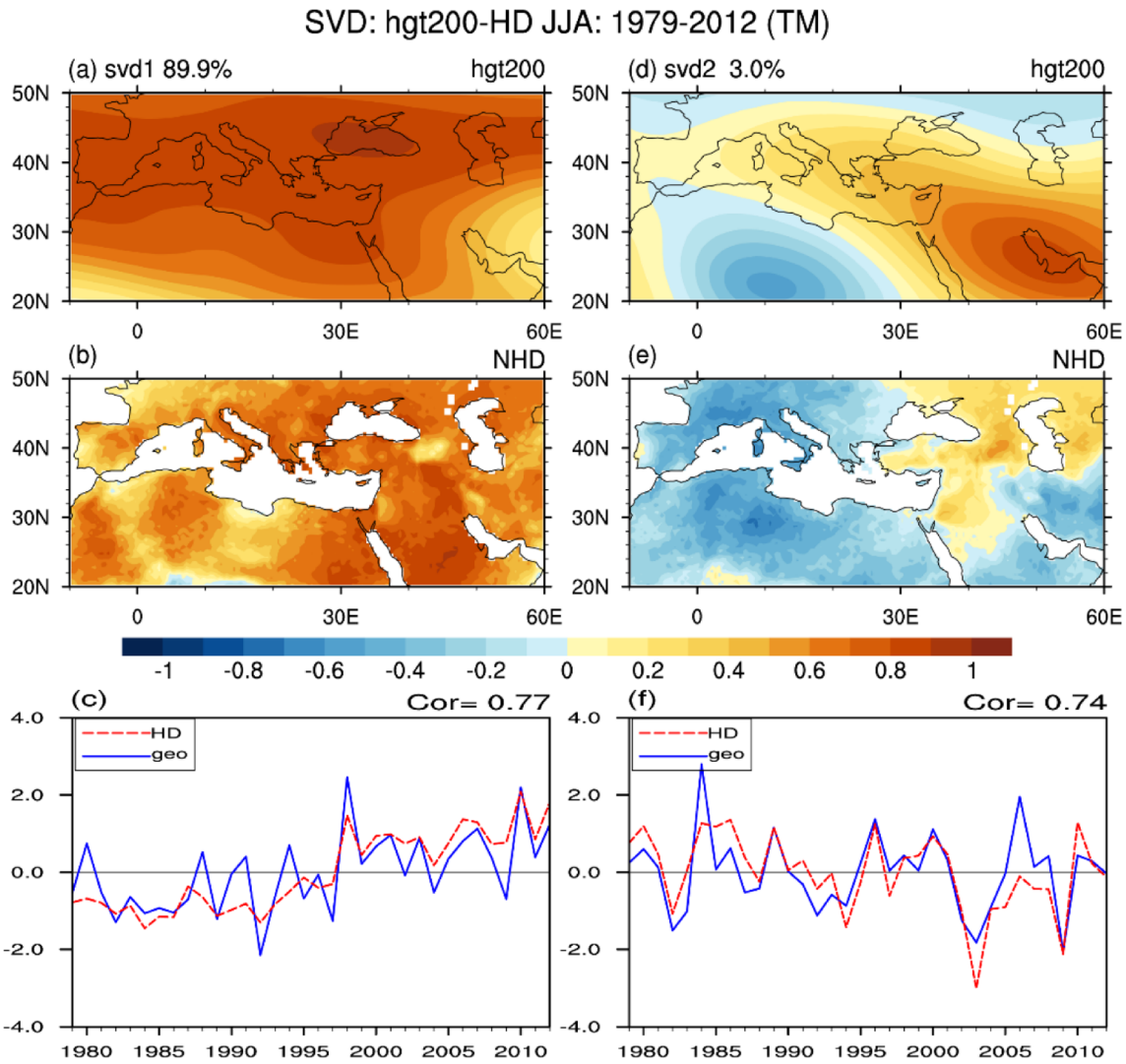

Fig. 10 **a**–**f** The same as Fig. 7 but over the TM region

To analyze the links between the general circulation and extreme temperature event over the USA, the first two SVD modes on summer 200 hPa geopotential height field and simultaneous NHD from 1979 to 2012 are shown in Fig. 13, and the first and second modes explain about 79.8% and 14.3% of the total variance, respectively.

The correlation coefficient between two corresponding PCs of geopotential height field and NHD from first mode is 0.82 (Fig. 13c), which suggests a close relationship between geopotential height field and NHD. As Fig. 13a, b shows, the first homogeneous SVD modes are characterized by uniform geopotential height fields and NHD anomalies in the USA region. NHD is above normal when the USA is controlled by an anomalous anticyclone. The standardized PCs of the first mode display a significant inter-annual variation with an increasing trend (Fig. 13c). The second mode indicates a dipole anomaly of 200 hPa geopotential height and NHD between the Northern and Southern USA. The correlation coefficient of PCs is 0.75, and the inter-annual variability of PCs is significant with a decreasing trend (Fig. 13f).

In the EA and TM, the NHD increased significantly with a regime shift around the late 1990s, but the NHD in the USA increased with significant inter-annual variability. Both the decadal increases of NHD in EA and north part of TM and positive anomalies NHD in the USA are associated with an anomalous anticyclone in both upper and lower troposphere, resulting subsidence at 500 hPa and downward shortwave radiation anomalies in the surface.

5 Discussion and conclusion

In this study, we have investigated the changes of high-temperature extremes and their links with atmospheric

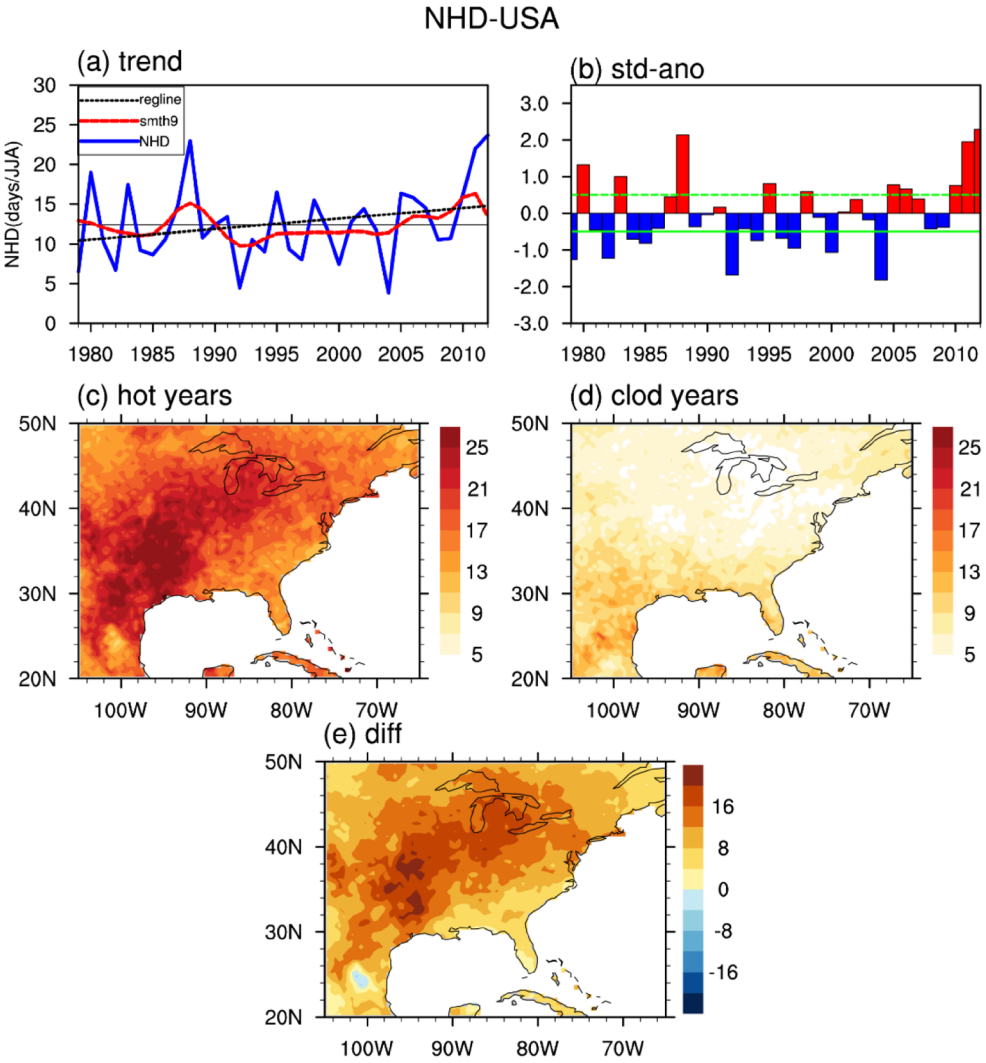

Fig. 11 Changes (**a**) and standardized anomalies (**b**) of regional averaged NHD based on percentile index during 1979–2012 and averaged NHD during hot years (**c**), cold years (**d**), and difference between hot years and cold years (**e**) in the USA region

circulation over the Northern Hemisphere during 1979–2012 based on daily records of maximum temperature and geopotential height fields. Hot day is defined as daily maximum temperature exceeding 35 °C (absolute index) or 90th percentile (percentile index) based on 30-year (1981–2010) daily records of daily maximum temperature.

Based on absolute index, the regions with frequent hot days are mainly located in the North Africa and West Asia, with the NHD close to 90 days/JJA. The spatial features of TX90 indicate a zonal structure and are consistent with the climatology of NHD based on absolute index, with larger values over the subtropical regions. The NHD increased with regional characteristics in most part of the Northern Hemisphere from 1979 to 2012 and had most significant increasing trends over the subtropical regions, especially around the Mediterranean. According to the features of climatology and trend, three sub-regions are chosen to do more detailed analysis: East Asia (EA), Mediterranean (TM), and United States of America (USA). These three regions are the areas where high-temperature extremes frequently occur and have significant increasing trends. In addition, the first EOF mode is characterized by a uniform increasing trend, with significant variations over the EA, TM, and USA.

In the EA region, regional NHD increased with a linear trend of 0.18 days/year, and showed a decadal increasing with a regime shift in 1996. Compared with the pre-period (1979–1996), hot days occur more frequently during the post-period (1997–2012), especially in the Mongolian Plateau and Loess Plateau. The atmospheric circulation and surface downward shortwave radiation associated with the decadal increasing of regional NHD are characterized by an anomalous anticyclone both in the upper and lower troposphere and the subsidence due to high pressure. This circulation pattern is conducive to the occurrence of hot days through enhancing downward solar radiation at the surface.

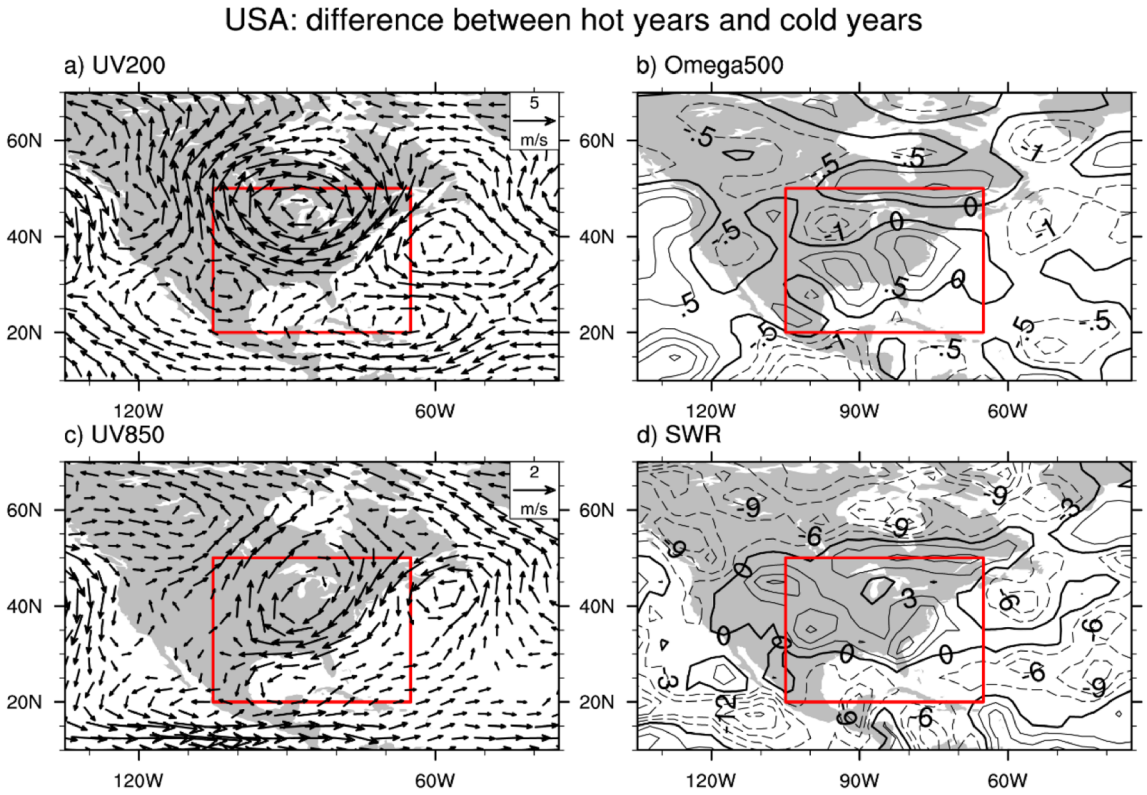

Fig. 12 Differences of (**a**) 200-hPa wind (units: m/s), (**b**) 500-hPa vertical pressure velocity (dp/dt) (units: 10^{-4} hPa/s), (**c**) 850-hPa wind (units: m/s), and (**d**) surface downward shortwave radiation (units: W/m^2) between hot years and cold years in the USA region. The red rectangular boxes denote the regions that are chosen as USA

In the TM region, regional NHD increased with a rate of 0.35 days/year and showed a decadal increasing with a regime shift in 1997. Factors associated with this shift are different over the north part and south part of TM. For the north part (from 40° N to north), the anomalous anticyclone and subsidence are responsible for the extreme temperature through enhancing solar radiation at surface. For the south part (from 40° N to south), there is no obvious anomalous anticyclone, but there are anomalous ascending and negative anomalous solar radiation at surface.

In the USA region, regional NHD increased with a linear trend of 0.1 days/year, and displayed an interannual variation. After defining hot years when the standardized anomaly of regional NHD is larger than 1.0, and cold years when the standardized is smaller than − 1.0, we chose 10 hot years and 10 cold years to do a composite analysis. Anticyclone and subsidence anomalies are conducive to the occurrence of hot years.

Anticyclonic anomalies play an important role in affecting extreme heat events in various regions from the previous studies (Meehl and Tebaldi 2004; Gershunov et al. 2009; Chen and Lu 2015). Subsidence resulting from anomalous anticyclone can increase the air temperature through adiabatic heating and also through enhancing solar radiation at surface due to the subsidence and reducing of cloud cover (Zaitchik et al. 2006; Loikith and Broccoli 2012). The decadal increasing over both the EA region and north part of TM region and also hot years over the USA region can be explained by mechanism mentioned above, but not the decadal increasing over south part of TM region.

Else, several previous studies indicated that the horizontal flow is responsible for extreme temperature through temperature advection over Mediterranean region. July–August temperature was analyzed over the eastern Mediterranean region (Ziv et al. 2004). The results indicated that the temperature anomaly is resulted from the combined effect of horizontal clod advection by prevailing northwesterly winds and the warming due to subsidence, and they tend to balance each other. In addition, Harpaz et al. (2014) did dynamical analysis of extreme summer temperatures in the east Mediterranean and implied that extreme heat is controlled by the intensity of the negative temperature advection, but not by the prevailing subsidence: high temperature is caused by the reducing of cold advection because of the weakened northwesterly wind.

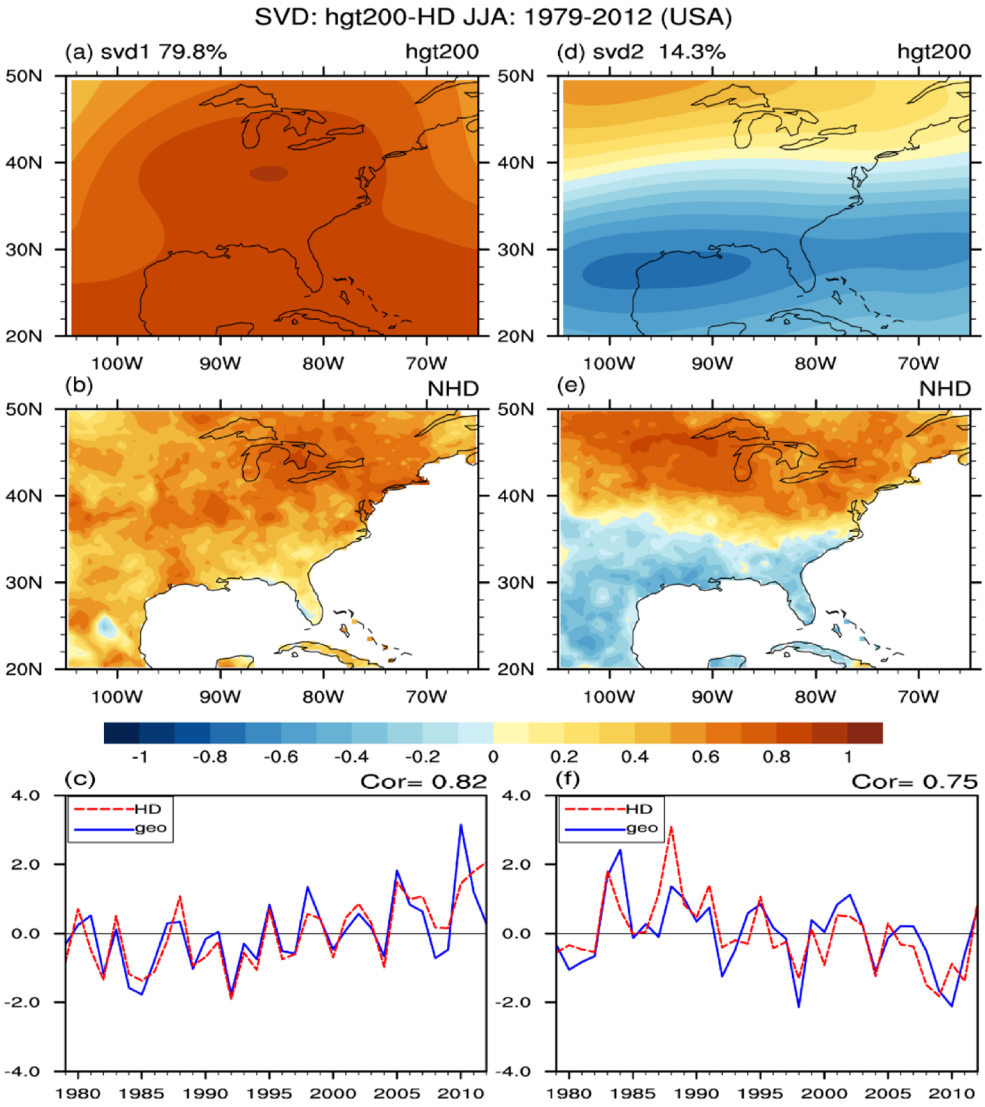

Fig. 13 **a**–**f** The same as Fig. 7 but over the USA region

Funding This work was supported by the National Natural Science Foundation of China (41425019, 41831175, and 41721004).

References

Alexander LV, Zhang X, Peterson TC, Caesar J, Gleason B, Tank A, ... Vazquez-Aguirre JL (2006). Global observed changes in daily climate extremes of temperature and precipitation. J Geophys Res-Atmos, 111(D5). doi: https://doi.org/10.1029/2005jd006290

Battisti DS, Naylor RL (2009) Historical warnings of future food insecurity with unprecedented seasonal heat. Science 323(5911):240–244. https://doi.org/10.1126/science.1164363

Black E, Blackburn M, Harrison G, Hoskins B, Methven J (2004) Factors contributing to the summer 2003 European heatwave. Weather 59 (8):217–223. https://doi.org/10.1256/wea.74.04

Bouchama A (2004) The 2003 European heat wave. Intensive Care Med 30(1):1–3

Chen R, Lu R (2015) Comparisons of the circulation anomalies associated with extreme heat in different regions of Eastern China. J Clim 28(14):5830–5844. https://doi.org/10.1175/jcli-d-14-00818.1

Choi G, Collins D, Ren G, Trewin B, Baldi M, Fukuda Y, Afzaal M, Pianmana T, Gomboluudev P, Huong PTT, Lias N, Kwon WT, Boo KO, Cha YM, Zhou Y (2009) Changes in means and extreme events of temperature and precipitation in the Asia-Pacific network region, 1955-2007. Int J Climatol 29(13):1906–1925. https://doi.org/10.1002/joc.1979

Coumou D, Rahmstorf S (2012) A decade of weather extremes. Nat Clim Chang 2(7):491–496. https://doi.org/10.1038/nclimate1452

Dee DP, Uppala S (2009) Variational bias correction of satellite radiance data in the ERA-Interim reanalysis. Q J R Meteorol Soc 135(644): 1830–1841. https://doi.org/10.1002/qj.493

Dee DP, Uppala SM, Simmons AJ, Berrisford P, Poli P, Kobayashi S, Andrae U, Balmaseda MA, Balsamo G, Bauer P, Bechtold P, Beljaars ACM, van de Berg L, Bidlot J, Bormann N, Delsol C, Dragani R, Fuentes M, Geer AJ, Haimberger L, Healy SB, Hersbach H, Hólm EV, Isaksen L, Kållberg P, Köhler M, Matricardi M, McNally AP, Monge-Sanz BM, Morcrette JJ, Park BK, Peubey C, de Rosnay P, Tavolato C, Thépaut JN, Vitart F (2011) The ERA-Interim reanalysis: configuration and performance of the data assimilation system. Q J R Meteorol Soc 137(656):553–597. https://doi.org/10.1002/qj.828

Diaz J, Garcia R, de Castro FV, Hernandez E, Lopez C, Otero A (2002) Effects of extremely hot days on people older than 65 years in

Seville (Spain) from 1986 to 1997. Int J Biometeorol 46(3):145–149. https://doi.org/10.1007/s00484-002-0129-z

Dole R, Hoerling M, Perlwitz J, Eischeid J, Pegion P, Zhang T, Quan XW, Xu T Murray D (2011). Was there a basis for anticipating the 2010 Russian heat wave? Geophys Res Lett, 38. doi: https://doi.org/10.1029/2010gl046582,

Dong B, Sutton RT, Shaffrey L (2016) Understanding the rapid summer warming and changes in temperature extremes since the mid-1990s over Western Europe. Clim Dyn 48:1–18. https://doi.org/10.1007/s00382-016-3158-8

Easterling DR, Meehl GA, Parmesan C, Changnon SA, Karl TR, Mearns LO (2000) Climate extremes: observations, modeling, and impacts. Science 289(5487):2068–2074. https://doi.org/10.1126/science.289.5487.2068

Gershunov A, Cayan DR, Iacobellis SF (2009) The great 2006 heat wave over California and Nevada: signal of an increasing trend. J Clim 22:6181–6203. https://doi.org/10.1175/2009JCLI2465.1

Gu S, Huang C, Bai L, Chu C, Liu Q (2016) Heat-related illness in China, summer of 2013. Int J Biometeorol 60(1):131–137. https://doi.org/10.1007/s00484-015-1011-0

Hansen J, Sato M, Ruedy R, Lo K, Lea DW, Medina-Elizade M (2006) Global temperature change. Proc Natl Acad Sci U S A 103(39):14288–14293. https://doi.org/10.1073/pnas.0606291103

Harpaz T, Ziv B, Saaroni H, Beja E (2014) Extreme summer temperature in the East Mediterranean—dynamical analysis. Int J Climatol 34:849–862. https://doi.org/10.1002/joc.3727

Horton DE, Johnson NC, Singh D, Swain DL, Rajaratnam B, Diffenbaugh NS (2015) Contribution of changes in atmospheric circulation patterns to extreme temperature trends. Nature 522(7557):465–469. https://doi.org/10.1038/nature14550

Hu L, Huang G, Hu K (2018) The performance of multiple datasets in characterizing the changes of extreme air temperature over China during 1979 to 2012. Theor Appl Climatol 133(1):619–632. https://doi.org/10.1007/s00704-017-2215-5

IPCC (2013). The physical science basis Contribution of Working Group I to the Fifth Assessment Report of the Intergovernmental Panel on Climate Change, ed T Stocker et al. Cambridge University Press, Cambridge

Kharin VV, Zwiers FW, Zhang X, Hegerl GC (2007) Changes in temperature and precipitation extremes in the IPCC ensemble of global coupled model simulations. J Clim 20(8):1419–1444. https://doi.org/10.1175/jcli4066.1

Kovats RS, Hajat S (2008) Heat stress and public health: a critical review. *Annu Rev Public Health* 29:41–55

Leechiong TL, Stitt JT (1995) Heatstroke and other heat-related illnesses—the maladies of summer. Postgrad Med 98(1):26–36

Loikith PC, Broccoli AJ (2012) Characteristics of observed atmospheric circulation patterns associated with temperature extremes over North America. J Clim 25:7266–7281. https://doi.org/10.1175/JCLI-D-11-00709.1

Luber G, McGeehin M (2008) Climate change and extreme heat events. Am J Prev Med 35(5):429–435. https://doi.org/10.1016/j.amepre.2008.08.021

Meehl GA, Tebaldi C (2004) More intense, more frequent, and longer lasting heat waves in the 21st century. Science 305(5686):994–997. https://doi.org/10.1126/science.1098704

Mitchell TD, Jones PD (2005) An improved method of constructing a database of monthly climate observations and associated high-resolution grids. Int J Climatol 25(6):693–712. https://doi.org/10.1002/joc.1181

Peng SB, Huang JL, Sheehy JE, Laza RC, Visperas RM, Zhong XH, ... Cassman KG (2004). Rice yields decline with higher night temperature from global warming. Proc Natl Acad Sci U S A, 101(27), 9971–9975. doi: https://doi.org/10.1073/pnas.0403720101

Perkins SE, Pitman AJ, Sisson SA (2013) Systematic differences in future 20 year temperature extremes in AR4 model projections over Australia as a function of model skill. Int J Climatol 33(5):1153–1167. https://doi.org/10.1002/joc.3500

Rodionov SN (2004) A sequential algorithm for testing climate regime shifts. Geophys Res Lett 31:L09204. https://doi.org/10.1029/2004GL019448

Schar C, Jendritzky G (2004) Climate change: hot news from summer 2003. Nature 432(7017):559–560. https://doi.org/10.1038/432559a

Valor E, Meneu V, Caselles V (2001) Daily air temperature and electricity load in Spain. J Appl Meteorol 40(8):1413–1421

Weedon GP, Balsamo G, Bellouin N, Gomes S, Best MJ, Viterbo P (2014) The WFDEI meteorological forcing data set: WATCH Forcing Data methodology applied to ERA-Interim reanalysis data. Water Resour Res 50(9):7505–7514. https://doi.org/10.1002/2014wr015638

Weedon GP, Gomes S, Viterbo P, Shuttleworth WJ, Blyth E, Oesterle H, ... Best M (2011). Creation of the WATCH Forcing Data and its use to assess global and regional reference crop evaporation over land during the twentieth century. J Hydrometeorol, 12(5), 823–848. doi: https://doi.org/10.1175/2011jhm1369.1

WMO (2013). The global climate 2001–2010: a decade of climate extremes. World Meteorological Organization Rep. 1103, 119pp. (Available online at https://library.wmo.int/pmb_ged/wmo_1119_en.pdf)

You Q, Kang S, Aguilar E, Pepin N, Fluegel W-A, Yan Y et al (2011) Changes in daily climate extremes in China and their connection to the large scale atmospheric circulation during 1961-2003. Clim Dyn 36(11–12):2399–2417. https://doi.org/10.1007/s00382-009-0735-0

Zaitchik BF, Macalady AK, Bonneau LR, Smith RB (2006) Europe's 2003 heat wave: a satellite view of impacts and land-atmosphere feedbacks. Int J Climatol 26:743–769. https://doi.org/10.1002/joc.1280

Zhao Y, Ducharne A, Sultan B, Braconnot P, and Vautard R (2015). Estimating heat stress from climate-based indicators: present-day biases and future spreads in the CMIP5 global climate model ensemble. Environ Res Lett, 10(8). doi: https://doi.org/10.1088/1748-9326/10/8/084013

Zhao Y, Sultan B, Vautard R, Braconnot P, Wang HJ, Ducharne A (2016) Potential escalation of heat-related working costs with climate and socioeconomic changes in China. Proc Natl Acad Sci U S A 113(17):4640–4645. https://doi.org/10.1073/pnas.1521828113

Ziv B, Saaroni H, Alpert P (2004) The factors governing the summer regime of the eastern Mediterranean. Int J Climatol 24:1859–1871. https://doi.org/10.1002/joc.1113